Received: 12 September 2025 | Accepted: 9 March 2026

DOI: 10.1002/hem3.70357

HemaSphere eha

ARTICLE

Integration of circulating tumor DNA profiling in the risk stratification of classical Hodgkin lymphoma in children, adolescents, and young adults

Mathieu Simonin[1] | Mathieu Viennot[2] | Stéphanie Haouy[3] | Stéphane Ducassou[4] | Catherine Curtillet[5] | Nathalie Garnier[6] | Aurélie Phulpin[7] | Catherine Paillard[8] | Charlotte Rigaud[9] | Marie-Laure Couec[10] | Liana Carausu[11] | Jacinthe Bonneau[12] | Isabelle Pellier[13] | Melissa Barbati[14] | Frédéric Millot[15] | Marie-Émilie Dourthe[16] | Justina Kanold[17] | Pascale Schneider[18] | Jean-Louis Stephan[19] | Camille Leglise[20] | Claire Pluchart[21] | Pierre-Julien Viailly[2] | Victor Michel[2] | Sabah Boudjemaa[22] | Bénédicte Jonca[23] | Thierry Leblanc[15] | Judith Landman-Parker[1] | Fabrice Jardin[2]

Graphical Abstract

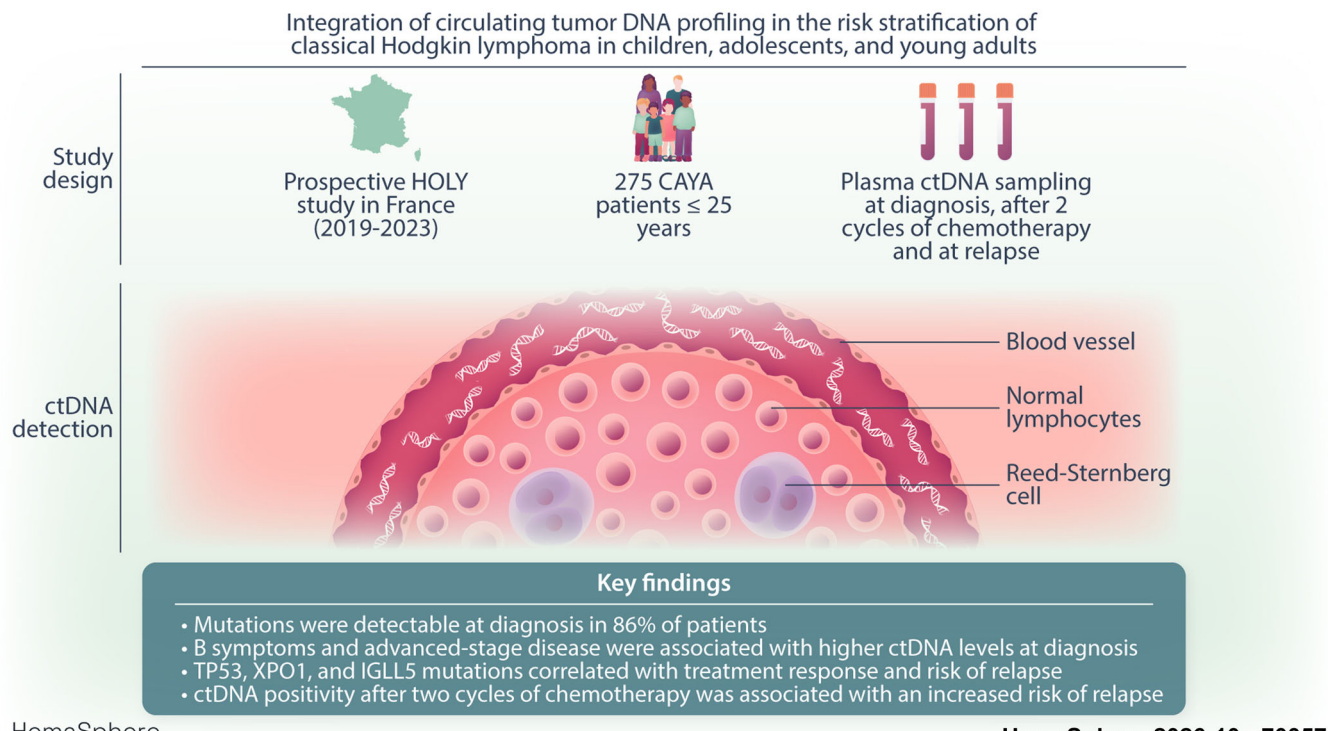

Received: 12 September 2025 | Accepted: 9 March 2026

DOI: 10.1002/hem3.70357

ARTICLE

HemaSphere eha

Integration of circulating tumor DNA profiling in the risk stratification of classical Hodgkin lymphoma in children, adolescents, and young adults

Mathieu Simonin[1] | Mathieu Viennot[2] | Stéphanie Haouy[3] | Stéphane Ducassou[4] | Catherine Curtillet[5] | Nathalie Garnier[6] | Aurélie Phulpin[7] | Catherine Paillard[8] | Charlotte Rigaud[9] | Marie-Laure Couec[10] | Liana Carausu[11] | Jacinthe Bonneau[12] | Isabelle Pellier[13] | Melissa Barbati[14] | Frédéric Millot[15] | Marie-Émilie Dourthe[16] | Justina Kanold[17] | Pascale Schneider[18] | Jean-Louis Stephan[19] | Camille Leglise[20] | Claire Pluchart[21] | Pierre-Julien Viailly[2] | Victor Michel[2] | Sabah Boudjemaa[22] | Bénédicte Jonca[23] | Thierry Leblanc[15] | Judith Landman-Parker[1] | Fabrice Jardin[2]

Correspondence: Mathieu Simonin (mathieu.simonin@aphp.fr) and Fabrice Jardin (fabrice.jardin@chb.unicancer.fr)

Abstract

This study aimed to define the potential role of circulating tumor DNA (ctDNA) in children, adolescents, and young adults (CAYA) with classical Hodgkin lymphoma (cHL). This prospective trial was conducted in France between 2019 and 2023 and recruited CAYA patients (≤25 years old) with a new diagnosis of cHL. Patients were treated according to the EuroNet-PHL-C2 trial (EudraCT: 2012-004053-88), and plasma ctDNA evaluations were performed at diagnosis, after two cycles of chemotherapy, and in case of relapse. Two hundred and seventy-five patients were included. Median age at diagnosis was 15 years (range 2–22), and 47% of the patients were treated as advanced stages (treatment level 3 [TL-3]). Using an 18-gene amplicon-based next-generation sequencing (NGS) targeted panel encompassing the most frequently mutated genes in cHL, at least one mutation was detected in 236/275 patients (86%). B-symptoms, erythrocyte sedimentation rate, and advanced stages were significantly associated with the level of ctDNA at diagnosis. *TP53* mutations (19/275, 7%) were strongly associated with inadequate response at early response assessment. *XPO1 and IGLL5* mutations were associated with a higher risk of relapse. The presence of detectable ctDNA after two cycles of chemotherapy (10%) was a strong and independent prognostic marker of relapse.

[1]Department of Pediatric Hematology and Oncology, Armand Trousseau University Hospital, AP-HP, Sorbonne Université, Paris, France
[2]Department of Hematology, Center Henri Becquerel, University of Rouen, INSERM UMR1245, Rouen, France
[3]Department of Pediatric Oncology and Haematology, University Hospital of Montpellier, Montpellier, France
[4]Department of Pediatric Oncology and Haematology, University Hospital of Bordeaux, Bordeaux, France
[5]Department of Pediatric Hematology and Oncology, APHM, La Timone Hospital, Marseille, France
[6]Institute of Pediatric Hematology and Oncology, Hospices Civils de Lyon, Lyon, France
[7]Pediatric Oncology and Hematology Department, University Hospital of Nancy (CHRU Nancy), Nancy, France
[8]Department of Pediatric Hematology and Oncology, Hautepierre University Hospital, Strasbourg, France
[9]Departments of Pediatric and Adolescent Oncology, Gustave Roussy, Université Paris-Saclay, Villejuif, France
[10]Pediatric Hematology and Oncology Department, University Hospital of Nantes, Nantes, France
[11]Department of Pediatric Hematology and Oncology, Centre Hospitalo-Universitaire de Brest, Brest, France
[12]Department of Pediatric Hematology and Oncology, Rennes University Hospital, Rennes, France

INTRODUCTION

Classical Hodgkin lymphoma (cHL) is the predominant lymphoma subtype in children, adolescents, and young adults (CAYA), comprising 15%–25% of all lymphomas.[1] Modern treatment approaches combining multi-modal chemotherapy and precision radiation techniques have transformed cHL into a highly curable malignancy, with 5-year survival rates exceeding 95% in this population.[2] Despite these advances, approximately 10% of patients develop recurrent or primary refractory disease, requiring intensive salvage therapy including radiation and/or high-dose chemotherapy with hematopoietic stem cell transplantation (HD-SCT), resulting in substantial treatment-related morbidity.[3] Conversely, while the majority of patients currently receive intensive front-line chemotherapy, some could achieve excellent outcomes with less intensive treatment approaches. These clinical challenges highlight two critical needs: identifying high-risk patients who may benefit from early therapeutic intervention, particularly novel approaches such as checkpoint inhibitors (CPI), and recognizing low-risk patients who could be candidates for treatment de-escalation to reduce the burden of treatment, minimize long-term complications, while maintaining excellent outcomes. The molecular characterization of cHL has been historically challenging due to the rarity of Hodgkin and Reed-Sternberg (HRS) cells, which constitute merely 0.1%–1% of the tumor microenvironment (TME), significantly hindering in vitro and ex vivo studies of malignant cell biology.[4,5] A significant breakthrough in cHL research occurred with the discovery of circulating tumor DNA (ctDNA) in blood plasma.[6] This approach has revolutionized the field by providing direct access to tumor-derived genetic material, revealing unprecedented insights into HRS cell genetics. The critical questions now focus on ctDNA's potential as an initial stratification biomarker and its utility for real-time treatment response monitoring. While ctDNA analysis has been extensively investigated in adult cHL patients with promising results, its application in CAYA has been restricted to small cohort studies.[6–13] We present a comprehensive national multicenter study examining the prognostic and predictive value of ctDNA monitoring in the largest pediatric cHL cohort assembled to date.

MATERIAL AND METHODS

Patients and patients' specimens

This prospective, observational study involved the collection of peripheral blood (PB) samples and clinical data from CAYA with cHL treated in France between December 2019 and January 2023 as part of an add-on study to the EuroNet-PHL-C2 trial (EudraCT: 2012-004053-88) in France.

Following the EuroNet-PHL-C2 trial's completion in December 2020, patients were treated according to updated French National Lymphoma Board guidelines that incorporated early EuroNet-PHL-C2 results while preserving the EuroNet-PHL-C2 chemotherapy backbone (Supporting Information S1: Figures 1–3).

Patients were eligible for inclusion if they had a confirmed cHL diagnosis, available biological samples, and provided signed informed consent. A total of 275 patients met these criteria and were enrolled. Subtyping of cHL was performed according to the World Health Organization Classification of Tumours of Hematopoietic and Lymphoid Tissues.[14] The biological material analyzed included ctDNA isolated from plasma samples collected at diagnosis, before treatment initiation. Paired ctDNA samples were also analyzed during treatment (after two cycles of OEPA: vincristine, etoposide, prednisone, and doxorubicin), corresponding to Day 1 of Cycle 3 (D1C3) and, if applicable, at relapse. Treatment decisions were made according to the EuroNet-PHL-C2 guidelines and were not modified based on ctDNA results obtained at diagnosis and at D1C3.

The study was conducted in accordance with French law and the principles of the Declaration of Helsinki. Ethical approval was obtained from the appropriate ethics committee, and written informed consent was obtained from all participants before inclusion.

DNA extraction and quantification

Cell-free DNA (cfDNA), defined as circulating DNA comprising both tumor-derived and non-tumor DNA, was extracted from 0.6 to 5.4 mL of plasma (median [Q1–Q3]: 3.0 mL [3.0–3.0]) using the QIAamp Circulating Nucleic Acid Kit (Qiagen, Hilden, Germany). cfDNA extracts were quantified using the Qubit dsDNA High Sensitivity Kit (Thermo Fisher Scientific, Waltham, MA, USA), yielding concentrations ranging from 0.3 to 27.6 ng/μL (median [Q1–Q3]: 2.01 [1.45–2.99] ng/μL). The mean plasma volumes (min–max) were 2.79 mL (0.6–4.6 mL) at baseline, 3.21 mL (1.5–5.4 mL) at D1C3, and 3.06 mL (2.5–4.6 mL) at relapse. For library preparation, 6.2–200 ng of cfDNA was used per sample (median [Q1–Q3]: 32.4 [27.9–44.6] ng). ctDNA, which refers specifically to the tumor-derived fraction of cfDNA, concentrations were expressed as haploid genome equivalents per milliliter of plasma (hGE/mL) and calculated by multiplying the mean variant allele frequency (VAF) across all mutations used for detection by the cfDNA concentration (pg/mL of plasma) and dividing by 3.3, assuming that one haploid genomic equivalent corresponds to 3.3 pg of DNA, as previously described by Scherer et al.[15] ctDNA values were log10-transformed to approximate a normal distribution for statistical analyses.

Library preparation

cfDNA libraries were constructed using the QIAseq Targeted DNA Panel kit (Qiagen) following the manufacturer's protocol. Briefly, cfDNA ends were repaired, followed by adapter ligation. These adapters contain the UMIs and the sample index. After the ligation step, a double clean was performed using QIAseq beads. Enrichment

[13]Pediatric Immuno-Hemato-Oncology, Angers University Hospital, CRCI2NA, UMR Inserm CNRS, Université d'Angers, Université de Nantes, Angers, France
[14]Department of Pediatric Hematology-Oncology, CHRU Lille, Lille, France
[15]Department of Pediatric Hematology-Oncology, CHU Poitiers, Poitiers, France
[16]Department of Pediatric Hematology and Immunology, Robert Debré University Hospital, AP-HP and Université de Paris, Paris, France
[17]Department of Pediatric Hematology-Oncology, University Hospital of Clermont-Ferrand, Clermont-Ferrand, France
[18]Pediatric Hematology, Immunology, Oncology and Stem Cells Transplantation, Rouen University Hospital Charles Nicolle CHU Rouen, Rouen, France
[19]Department of Pediatrics, Centre Hospitalier Universitaire Saint-Etienne, Saint-Priest en Jarez, France
[20]Department of Pediatric Oncology, Hematology, Immunology, University Hospital of Amiens, Amiens, France
[21]Pediatric Oncology and Hematology Department, Reims University Hospital, Reims, France
[22]Pathology Department, Armand Trousseau University Hospital, AP-HP, Sorbonne Université, Paris, France
[23]Department of Nuclear Medicine, University Hospital Tenon, Paris, France

was then performed using primers targeting 18 genes previously described as frequently mutated in cHL. Following enrichment, a clean-up was performed, followed by universal polymerase chain reaction (PCR). After this last PCR, a final clean-up was performed.

Sequencing

Quantification of the purified libraries was performed using the Qubit dsDNA High Sensitivity kit. Sequencing was performed with the NextSeq. 550 System (Illumina, San Diego, CA, USA) to manufacturer's recommendations using paired-end sequencing (2 × 150 bp) with the NextSeq. 550 High Output Kit v2.5.

Data analysis and statistical methods

Post-sequencing analysis of the FASTQ files was performed using two pipelines, Genomics Workbench v. 21.0.3 (Qiagen) with the Biomedical Genomics Analysis Plugin v. 21.0.1, and a local solution using BWA v. 0.7.17, UMI-VarCal,[16] and GenerateReports (Genexpath, Rouen, France).

To analyze the results, the variant calling files were combined and the variants were filtered using a semi-automatic analysis in R. Finally, each variant was confirmed by visual inspection employing the Integrative Genomics Viewer software to exclude technical artifacts, including variants supported only by reads aligned to problematic genomic regions (e.g., GC-rich or repetitive regions), variants located at the ends of reads, variants supported exclusively by short reads, and variants supported by unpaired reads (i.e., present only in forward or reverse reads when a match was expected). Our panel was not specifically designed for the detection of phased variants (PVs), but PVs were nevertheless identified in a subgroup of patients. For this subgroup, for D1C3 and relapse samples, supervised variant calling using the UMI-VarCal whitelist feature was performed for each patient with PVs identified at baseline.[17] UMI-VarCal estimates the PVs within a range of 135 base pairs using UMI sequences. Variants were considered phased if they were carried by the same UMI. A minimum of three UMIs carrying these PVs was required to qualify them as tumor markers at diagnosis. At D1C3 and relapse, ctDNA was considered detectable if at least one somatic mutation was identified at baseline or a novel mutation was detected. ctDNA was considered undetectable when no baseline mutation or novel mutation was detected.

The detection threshold was defined on a per-sample basis, according to the estimated background error rate of each sequencing library, determined using Phred scores (Supporting Information S2: Tables 1–3).

Patient characteristics were compared using Fisher's exact test for categorical variables, and parametric (*t*-test) or non-parametric (Mann–Whitney *U* test or analysis of variance) tests for continuous variables, with significance set at $P < 0.05$. Survival analyses for overall survival (OS) and event-free survival (EFS) were performed using the log-rank test. OS was defined from diagnosis to death (censoring survivors at last follow-up), while EFS was defined from diagnosis to relapse or death. Univariate survival analysis used the Cox proportional hazards model, reporting hazard ratios (HRs) and 95% confidence intervals (CIs). To identify genetic predictors of EFS while avoiding overfitting with multiple correlated predictors, we performed LASSO (Least Absolute Shrinkage and Selection Operator) penalized Cox proportional hazards regression using the CoxNet algorithm. Seventeen recurrently mutated genes detected by ctDNA profiling at diagnosis were included as candidate predictors. The LASSO penalty (L1 regularization, $\alpha = 1$) was applied to perform automatic variable selection by shrinking coefficients of non-informative predictors to zero. The optimal regularization parameter (λ) was selected using 10-fold cross-validation, maximizing the concordance index (C-index).[18] Analyses were performed using R v4.3.0 and Python 3.11.7.

RESULTS

Plasma samples and cfDNA characteristics

Of the collected samples, 545 plasma specimens fulfilled the predefined quality and quantity criteria for next-generation sequencing (NGS) analysis, comprising 275 obtained at baseline, 250 at D1C3, and 20 at relapse.

Clinical characteristics of included CAYA patients with cHL

Clinical characteristics and disease features for the 275 patients with evaluable ctDNA at diagnosis are presented in Table 1. In this CAYA cHL cohort ($N = 275$), patients had a median age of 15 years (range: 2–22), with 45% male. Disease characteristics showed bulky disease in 37% and B-symptoms in 49% of cases. Advanced stages (III/IV) were observed in 49% of patients. Histologically, nodular sclerosis predominated (87%), followed by mixed cellularity (6%). Epstein–Barr virus (EBV)-positive HRS cells were detected in 15% of cases. Treatment allocation following EuroNet-PHL-C2 protocol stratification (Supporting Information S1: Figures 1 and 2) resulted in 13% of patients receiving treatment level 1 (TL-1), 40% TL-2, and 47% TL-3 therapy. At a median follow-up of 29 months (range: 27.8–32.9), the 30-month OS was 100%, and the 30-month EFS was 90% (95% CI: 86–94%) (Supporting Information S1: Figure 3).

Detection of somatic variants in pretreatment ctDNA of cHL CAYA patients

Using our targeted capture NGS panel covering 18 genes recurrently mutated in cHL, a total of 2282 somatic single-nucleotide variants (SNVs) and insertions/deletions (indels) were detected in 236 out of 275 diagnostic samples (86%). Among these cases, the number of variants per patient ranged from 1 to 54 (median: 9), with a VAF per patient ranging from 0.11% to 51.87% (median: 3.48%). Among patient with a detectable mutation, the median ctDNA concentration was 2.48 $\log_{10}$(hGE/mL) (range: 2.13–2.83). Eight of the 18 genes were recurrently mutated in more than 20% of cases. The most frequently altered genes included *SOCS1* (68%), *IGLL5* (44%), *B2M* (43%), *CIITA* (41%), *TNFAIP3* (37%), *STAT6* (32%), *NFKBIE* (31%), *ITPKB* (29%), and *GNA13* (21%) (Figure 1A). Regarding variant types, nonsynonymous SNVs were the most common (43%), followed by frameshift deletions (14%) and intronic mutations (11%) (Figure 1B). The mean VAF per gene was 5.7% (range: 3.7%–8.5%) (Figure 1C).

We observed that certain gene pairs rarely co-occurred: *NFKBIE* and *STAT6*, *NFKBIE* and *TNFAIP3*, *NFKBIE* and *ARID1A*, *PTPN1* and *STAT6*, *PTPN1* and *TNFAIP3*, and *ITPKB* and *ARID1A* (Figure 1D and Supporting Information S1: Figure 4).

Correlation between baseline cfDNA levels and disease characteristics

Among the 236 patients out of 275 with detectable ctDNA at diagnosis, ctDNA levels expressed in $\log_{10}$(hGE/mL) were significantly associated with several clinical and biological features (Table 2). Patients with a bulky mass had significantly higher ctDNA levels compared to those without;

TABLE 1 Clinical characteristics of patients stratified by circulating tumor DNA (ctDNA) detection status at diagnosis.

	ctDNA at diagnosis			
	Not detectable (*n* = 39)	Detectable (*n* = 236)	Total (*N* = 275)	P value
Median age, years (range)	14 (4–18)	15 (2–22)	15 (2, 22)	**<0.01**[a]
Male sex	19 (49%)	106 (45%)	125 (45%)	0.73[b]
B-symptoms	12/39 (31%)	122/234 (52%)	134/274 (49%)	**0.02**[b]
EBV-positive disease	10/27 (37%)	20/169 (12%)	30/196 (15%)	**<0.01**[b]
ESR ≥ 30 mm	20/36 (56%)	158/224 (71%)	178/260 (68%)	0.08[b]
Bulky disease (≥200 mL)	7/38 (18%)	93/233 (40%)	100/271 (37%)	**0.01**[b]
Ann Arbor stage	NA = 0	NA = 1	NA = 1	0.18[b]
I	2 (5%)	2 (1%)	4 (1%)	
II	20 (51%)	117 (50%)	137 (50%)	
III	10 (26%)	55 (23%)	65 (24%)	
IV	7 (18%)	61 (26%)	68 (25%)	
Advanced stages (III and IV)	17 (44%)	116 (49%)	133 (49%)	0.60[b]
Treatment level	NA = 0	NA = 1	NA = 1	**0.03**[b]
TL-1	10 (26%)	25 (11%)	35 (13%)	
TL-2	16 (41%)	93 (40%)	109 (40%)	
TL-3	13 (33%)	117 (50%)	130 (47%)	
Treatment		NA = 9	NA = 9	0.30[c]
OEPA X2	2 (5%)	4 (2%)	6 (2%)	
OEPA X2 + COPDAC 28	7 (18%)	23 (10%)	30 (11%)	
OEPA X2 + COPDAC 28 X2	13 (33%)	62 (26%)	75 (27%)	
OEPA X2 + COPDAC 28 X4	7 (18%)	61 (26%)	68 (25%)	
OEPA X2 + DECOPDAC 21 X2	4 (10%)	30 (13%)	34 (12%)	
OEPA X2 + DECOPDAC 21 X4	6 (15%)	47 (20%)	53 (19%)	
Histology	NA = 3	NA = 19	NA = 22	**<0.01**[b]
Nodular sclerosis	24 (67%)	196 (90%)	220 (87%)	
Mixed cellularity	8 (22%)	6 (3%)	14 (6%)	
Others	4 (11%)	15 (7%)	19 (8%)	
OR at ERA	NA = 0	NA = 1	NA = 1	0.14[b]
Adequate response (DS ≤ 3)	30 (77%)	150 (64%)	180 (66%)	
Inadequate response (DS ≥ 4)	9 (23%)	85 (36%)	94 (34%)	
Event-free survival				**0.02**[c]
EFS at 12 months 95% CI	100% (100%–100%)	94% (90%, 97%)	94% (92%, 97%)	
EFS at 24 months 95% CI	100% (100%–100%)	91% (87%, 95%)	92% (89%, 95%)	

Note: P values < 0.05 are depicted in bold.

Abbreviations: DS, Deauville score; EBV, Epstein–Barr virus; EFS, event-free survival; ESR, erythrocyte sedimentation rate; NA, not available; OR at ERA, overall response at early response assessment by positron emission tomography-computed tomography (PET-CT); TL, treatment level.

[a]Wilcoxon test,

[b]Fisher's exact test,

[c]Log-rank test.

median $\log_{10}$(hGE/mL) = 2.63 versus 2.35; P < 0.001 (Figure 2A). The presence of B-symptoms was also associated with increased ctDNA levels (2.59 vs. 2.38; P < 0.01) (Figure 2B). Additionally, patients with an elevated erythrocyte sedimentation rate (ESR > 30 mm) had significantly higher ctDNA concentrations compared to those with a lower ESR (2.53 vs. 2.33; P < 0.01) (Figure 2C). Similarly, patients with advanced-stage disease (Stages III–IV) had higher ctDNA levels than those with early-stage disease (Stages I–II) (2.60 vs. 2.33; P < 0.01) (Figure 2D). Consistent with these findings, ctDNA levels correlated with treatment stratification according to the EuroNet-PHL-C2 protocol (Figure 2E and Supporting Information S1: Figure 1). In contrast, no significant differences in ctDNA concentration were observed based on sex, age at diagnosis, or EBV status.

Patients without detectable ctDNA at diagnosis (39/275, 14%) exhibited distinct clinical and biological features compared to those with detectable ctDNA (236/275, 86%). These patients were younger, had a

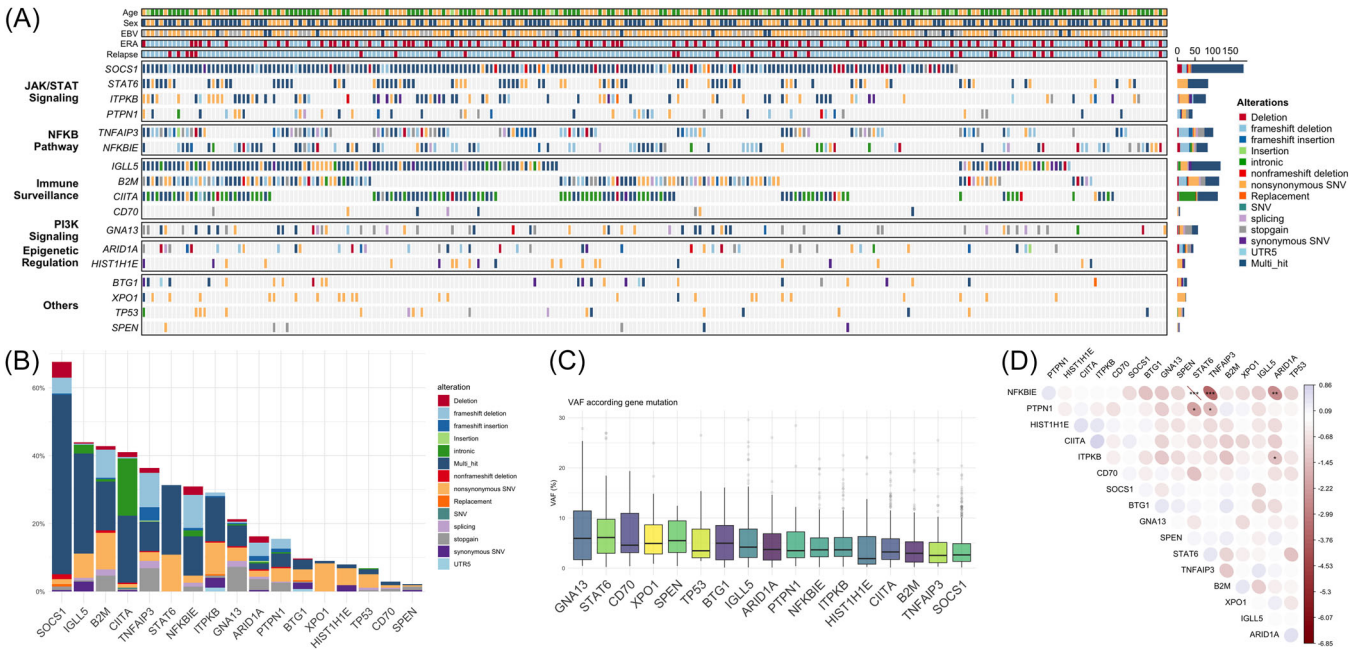

FIGURE 1 **Mutational landscape of pediatric classical Hodgkin lymphoma at diagnosis. (A)** Oncoplot displaying the mutational profile of 236 patients with pediatric classical Hodgkin lymphoma. **(B)** Stacked bar chart showing the mutation frequency (%) for each gene across the cohort. Bar height represents the proportion of patients harboring mutations in each gene, with colors indicating the distribution of alteration types. **(C)** Boxplots displaying the variant allele frequency (VAF, %) distribution for mutations in each gene. Boxes represent the interquartile range (IQR) with the median line; whiskers extend to 1.5× IQR. Genes are ordered by median VAF. **(D)** Correlation matrix showing pairwise co-mutation patterns between genes. Circle size and color intensity represent the strength and direction of association (log-transformed). Positive associations (co-occurrence) are shown in blue, and negative associations (mutual exclusivity) are shown in red.

lower incidence of bulky disease (17% vs. 40%; P < 0.01), and were less likely to present with B-symptoms (31% vs. 52%; P = 0.02) (Table 1). Biologically, patients without detectable ctDNA at diagnosis showed higher rates of EBV-positive cHL (37% vs. 12%; P < 0.01) and mixed cellularity histological subtype (22% vs. 3%; P < 0.01). Despite similar rates of advanced-stage disease (Stage III/IV: 44% vs. 49%; P = 0.6) and comparable inadequate response (IR) rates at early response assessment (ERA) by positron emission tomography-computed tomography (PET-CT) (Deauville score ≥ 4: 23% vs. 36%; P = 0.14), these patients demonstrated superior outcomes, with 30-month EFS of 100% versus 85% (P = 0.02, log-rank test).

Impact of ctDNA levels at diagnosis and ERA

Although baseline ctDNA levels were not significantly predictive of PET-CT response at ERA, a trend was observed: patients with IR at ERA had higher ctDNA levels at diagnosis compared to AR (median $\log_{10}$(hGE/mL): 2.55 vs. 2.46; P = 0.064) (Figure 2F).

In contrast, the ctDNA level at diagnosis was a significant predictor of volumetric tumor reduction evaluated by CT after two cycles of chemotherapy. Patients achieving ≥75% volumetric reduction at ERA had significantly lower baseline ctDNA levels than patients with 50 to 75% volumetric reduction (median $\log_{10}$(hGE/mL): 2.44 vs. 2.55; P = 0.017) (Figure 2G).

Impact of ctDNA detection after two cycles of chemotherapy

i. **Correlation between ctDNA at D1C3 and disease characteristics**

ctDNA assessment at D1C3 was available for 250 patients, including 217 of the 236 patients (92%) who had detectable ctDNA at diagnosis. Among these 217 patients, 23 (11%) still had detectable ctDNA at D1C3. Patients with persistent ctDNA at D1C3 had significantly higher ctDNA levels at diagnosis compared to those who cleared ctDNA; median $\log_{10}$(hGE/mL): 2.9 versus 2.4; P < 0.001. Persistent ctDNA at D1C3 was also more frequently associated with adverse clinical features, including bulky disease (57% vs. 35%; P = 0.04), advanced-stage disease (70% vs. 45%; P = 0.03), and the presence of B-symptoms at diagnosis (70% vs. 45%; P = 0.03) (Supporting Information S1: Figure 5).

ii. **Persistence of ctDNA at D1C3 as an independent predictor of relapse risk**

Patients with detectable ctDNA at D1C3 had significantly lower 30-month EFS, with an EFS rate of 67% (95% CI, 48–94), compared with 92% (95% CI, 88–96) in patients without detectable ctDNA (log-rank P < 0.001) (Figure 3A). Cox proportional hazards analysis demonstrated a 4.47-fold increased risk of events associated with ctDNA positivity at D1C3 (HR 4.47; 95% CI, 1.88–10.7; P < 0.001) (Figure 3A). Among the 23 patients with detectable ctDNA at D1C3: 15 patients (65%) were concordant with positive PET at ERA (ctDNA+/PET+), 8 patients (35%) were discordant with negative PET (ctDNA+/PET−) (Figure 3B,C and Supporting Information S1: Figure 6). Notably, among the 8 discordant patients (ctDNA+/PET−), one patient subsequently relapsed, indicating that ctDNA detected residual disease that was not identified by PET imaging. This case highlights the potential increased sensitivity of ctDNA monitoring for detecting minimal residual disease below the PET detection threshold. The remaining seven ctDNA+/PET− patients did not relapse, suggesting that while ctDNA may offer enhanced sensitivity, it may also detect low-level tumor DNA that does not

TABLE 2 Correlation between circulating tumor DNA (ctDNA) level and clinical and biological characteristics.

Characteristics	*N* 236 pts	Plasma ctDNA concentration log_{10}(hGE/mL) Median (Q1–Q3)	Range	P value
Sex				0.50
Male	106	2.42 (2.04–2.83)	0.82–4.03	
Female	130	2.50 (2.17–2.84)	1.15–3.73	
Age				0.75
<10 years	10	2.41 (2.09–2.84)	1.27–3.34	
10–14 years	85	2.51 (2.17–2.86)	1.15–4.03	
≥15 years	141	2.46 (2.10–2.81)	0.82–3.69	
ESR ≥ 30 mm				**0.002**
Yes	158	2.53 (2.18–2.96)	0.82–4.03	
No	66	2.33 (2.00–2.61)	1.27–3.37	
B-symptoms				**<0.01**
Yes	112	2.59 (2.23–3.15)	0.82–4.03	
No	122	2.38 (1.99–2.64)	1.15–3.35	
Bulky disease (≥200 mL)				**<0.01**
Yes	93	2.63 (2.31–3.12)	1.43–3.73	
No	140	2.35 (2.04–2.71)	0.82–4.03	
Ann Arbor stage				**<0.01**
I–II	119	2.33 (2.03–2.68)	0.82–3.73	
III–IV	116	2.60 (2.24–3.09)	1.38–4.03	
EBV-positive disease				0.24
Yes	20	2.59 (2.22–2.97)	1.62–4.03	
No	149	2.49 (2.15–2.78)	0.82–3.73	
Treatment level				**<0.01**
TL-1	25	2.23 (1.98–2.47)	1.27–3.12	
TL-2	93	2.42 (2.06–2.69)	0.82–3.73	
TL-3	117	2.63 (2.18–3.10)	1.38–4.03	
Histology				**0.03**
Nodular sclerosis	196	2.47 (2.14–2.82)	1.27–3.73	
Mixed cellularity	6	1.90 (1.47–2.42)	0.82–2.60	
Others	15	2.55 (2.15–3.19)	1.15–4.03	
Volumetric reduction at ERA				**0.017**
>75% volume reduction	*78*	2.44 (2.03–2.82)	0.82–4.03	
≤75% volume reduction	*109*	2.55 (2.18–3.00)	1.43–3.73	
Overall response at ERA				0.06
Adequate response (DS ≤ 3)	150	2.46 (2.07–2.75)	0.82–4.03	
Inadequate response (DS ≥ 4)	85	2.55 (2.20–3.00)	1.37–3.72	

Note: P values < 0.05 are depicted in bold.

Abbreviations: DS, Deauville score; EBV, Epstein–Barr virus; ERA, early response assessment evaluated by positron emission tomography-computed tomography (PET-CT); ESR, erythrocyte sedimentation rate; TL, treatment level.

necessarily translate into clinical outcome in all cases. These findings support the complementary value of ctDNA and metabolic imaging for early response assessment in pediatric Hodgkin lymphoma.

Importantly, in multivariate analysis adjusted for PET response at ERA, persistent ctDNA remained an independent predictor of inferior EFS (HR, 3.24; 95% CI, 1.3–7.9; P = 0.01) (Figure 3D). These findings underscore the prognostic significance of ctDNA persistence at D1C3 in identifying patients at the highest risk of relapse.

Prognostic value of somatic mutations identified at baseline in CAYA Hodgkin lymphoma

i. ***TP53* mutation is a strong predictor of IR after two cycles of chemotherapy**

Among the 236 patients with at least one mutation at diagnosis, 19 (8%) harbored a *TP53* mutation. Patients with *TP53* mutations were older than those with wild-type *TP53* (median age: 16 years [range: 11–22] vs. 15 years [range: 2–22]; P = 0.02). Notably, *TP53* mutations were not associated with advanced-stage disease, bulky mass, or the presence of B-symptoms. However, the presence of *TP53* mutations at diagnosis was strongly predictive of an IR at the ERA, with 68% (13/19) of *TP53*-mutated patients classified as IR compared to 32% among *TP53* wild-type patients (P = 0.002). Moreover, late response assessments (LRAs) evaluated by PET-CT at the end of treatment were also less favorable, with 60% of TP53-mutated patients exhibiting a Deauville score ≥ 4 compared with 22% of TP53 wild-type patients (P = 0.02). Despite these unfavorable early and late response indicators, TP53 mutations were not associated with a significantly increased risk of relapse.

ii. **Identification of *XPO1/IGLL5* mutations as an independent predictor of relapse**

We applied a penalized Lasso Coxnet regression model to assess the association between genetic mutations from our NGS panel and the risk of relapse. This analysis showed that *XPO1* and *IGLL5* alterations were significantly associated with an increased risk of relapse.

Patients harboring *XPO1* and/or I*GLL5* mutations (130/275, 47%) were associated with a significantly increased risk of relapse (HR, 3.65; 95% CI, 1.7–7.9; P < 0.001) (Figure 4A and Supporting Information S1: Figure 7). Importantly, in a multivariate Cox model adjusted for PET-CT response at ERA, *XPO1/IGLL5* status remained an independent predictor of relapse (HR, 2.69; 95% CI, 1.19-6.10; P = 0.018) (Figure 4B). These findings support a combined risk stratification model incorporating both PET-CT response and genetic alterations and ctDNA at D1C3. After integration of PET-CT evaluation at ERA, three distinct risk groups were identified (Figure 4C). Patients classified as low risk, defined by an AR at ERA and absence of XPO1/IGLL5 alterations, represented 37% of the cohort and had an EFS of 98% (95% CI, 95–100). High-risk patients, defined by an IR at ERA and presence of *XPO1/IGLL5* alterations, comprised 18% of the cohort and had an EFS of 79% (95% CI, 68–91). The remaining patients constituted an intermediate-risk group (45% of the cohort) with EFS of 87% (95% CI, 80–94).

To assess the independent prognostic value of these biomarkers, we performed multivariate Cox regression analysis including the three most relevant factors identified in our study—ctDNA detectability at D1C3, XPO1/IGLL5 mutation status, and IR at ERA—along with established prognostic variables (elevated ESR, advanced stage). In this model, ctDNA persistence at D1C3, IR at ERA, and XPO1/IGLL5 mutations remained independently associated with inferior EFS (Figure 4D).

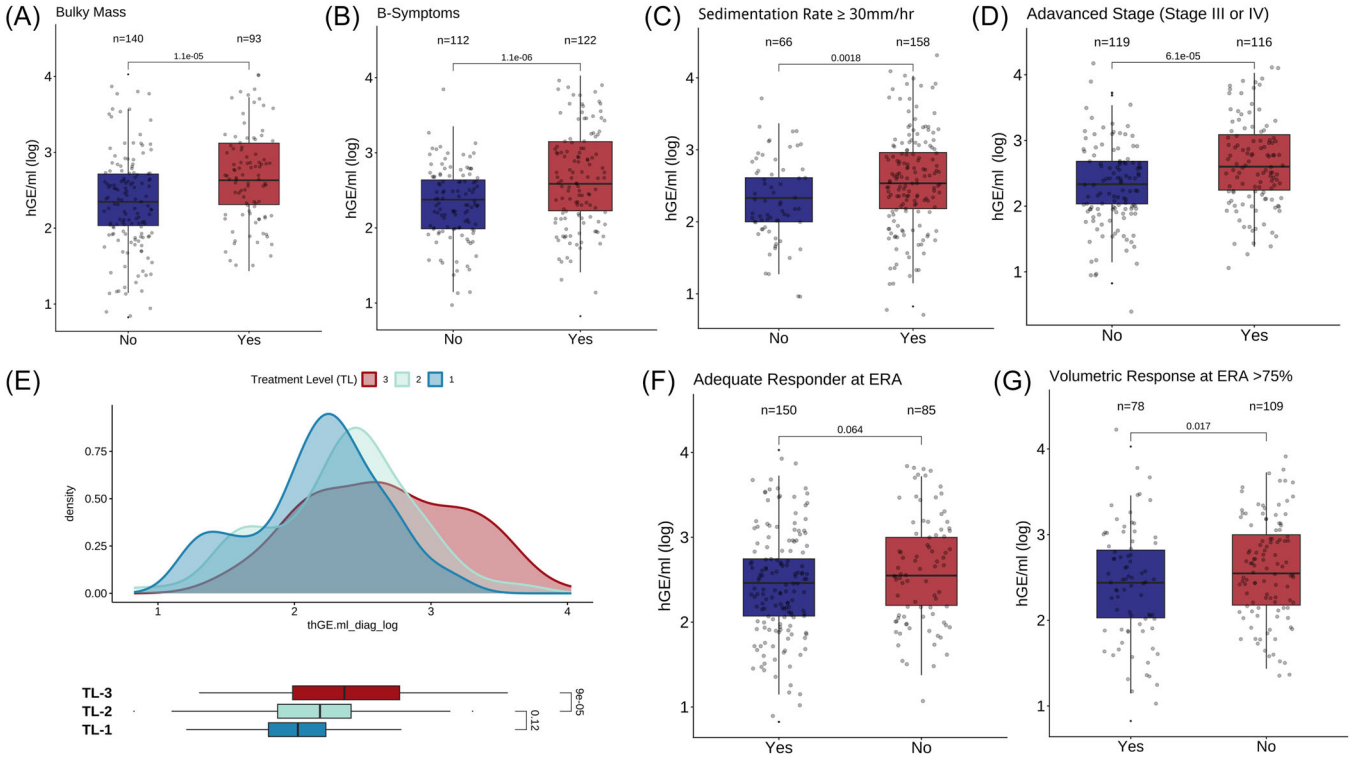

FIGURE 2 **Association between baseline circulating tumor DNA (ctDNA) levels and clinical characteristics at diagnosis. (A)** ctDNA levels according to bulky mass at diagnosis. **(B)** ctDNA levels according to B-symptoms at diagnosis. **(C)** ctDNA levels according to erythrocyte sedimentation rate (ESR) ≥ 30 mm/h at diagnosis. **(D)** ctDNA levels according to disease stage at diagnosis. **(E)** Density plot (top) and boxplot (bottom) showing the distribution of baseline ctDNA levels according to treatment level. Treatment level 3 (TL-3, red), TL-2 (light teal), and TL-1 (blue) are displayed. **(F)** ctDNA levels according to adequate response status at early response assessment (ERA). **(G)** ctDNA levels according to volumetric response (>75% reduction) at ERA.

Mutational evolution between diagnosis, at D1C3, and relapse

When considering all mutations collectively to define a specific gene alteration, we observed that among the 23 patients with persistent ctDNA at D1C3, 18 (78%) harbored a *TNFAIP3* mutation at diagnosis, with 12 of these patients losing this mutation at D1C3. Interestingly, *TP53* mutations at diagnosis were not associated with persistent ctDNA at D1C3; only two patients (9%) with detectable ctDNA at D1C3 had a *TP53* mutation at diagnosis, and these mutations were not detected at D1C3. The majority of mutations present at diagnosis were not detected at D1C3. Acquisition of new mutations at D1C3 was extremely rare; we detected only a single gain of an *XPO1* mutation in one patient (Figure 5A–C).

Overall, 29 patients out of 275 (10.5%) experienced disease relapse. Among these patients, we obtained ctDNA samples at the time of relapse for 20 individuals. Notably, only 14 of these 20 patients (70%) demonstrated persistently detectable ctDNA at relapse. Molecular analysis revealed that while the majority of mutations present at diagnosis were conserved at relapse, six patients (30%) acquired novel mutations between initial diagnosis and subsequent relapse, suggesting clonal evolution during treatment (Figure 5D).

DISCUSSION

In this study, we confirm the feasibility of noninvasive somatic mutation analysis in a large, prospective cohort of CAYA with cHL. We successfully identified mutations through NGS, even when targeting a limited panel of genes. Our investigation revealed recurrent mutations in plasma ctDNA across our cohort of 275 consecutive CAYA patients with cHL. Most significantly, we report for the first time the longitudinal molecular evolution during therapy and at relapse in the largest pediatric series documented to date. Notably, 86% of our CAYA cHL patients harbored detectable somatic mutations, confirming that ctDNA assessment represents a valuable approach for defining the molecular landscape of this disease at diagnosis.[11,19,20]

Previous studies have reported the potential role of ctDNA at diagnosis as a correlating or surrogate marker for disease burden, showing associations with inflammatory signs present at diagnosis. In our large cohort, we confirm significant associations between median ctDNA concentration at diagnosis and several clinical parameters including disease stage, ESR, and presence of bulky disease. These findings demonstrate a clear correlation between ctDNA levels and both tumor mass and the inflammatory response it generates. These results position ctDNA assessment at diagnosis as a promising new tool for disease stratification that could complement or potentially enhance current clinical staging approaches.

We identified a distinct subgroup of patients without detectable ctDNA at diagnosis (comprising 14% of the cohort), who exhibited specific clinical and biological features: younger age, EBV-driven disease, and mixed cellularity histology. Interestingly, these patients displayed a distribution of classical staging criteria comparable to those with detectable ctDNA, yet demonstrated better outcomes. Whether this finding reflects limited assay sensitivity or a biologically distinct subgroup characterized by low mutational burden and favorable prognosis remains to be determined.

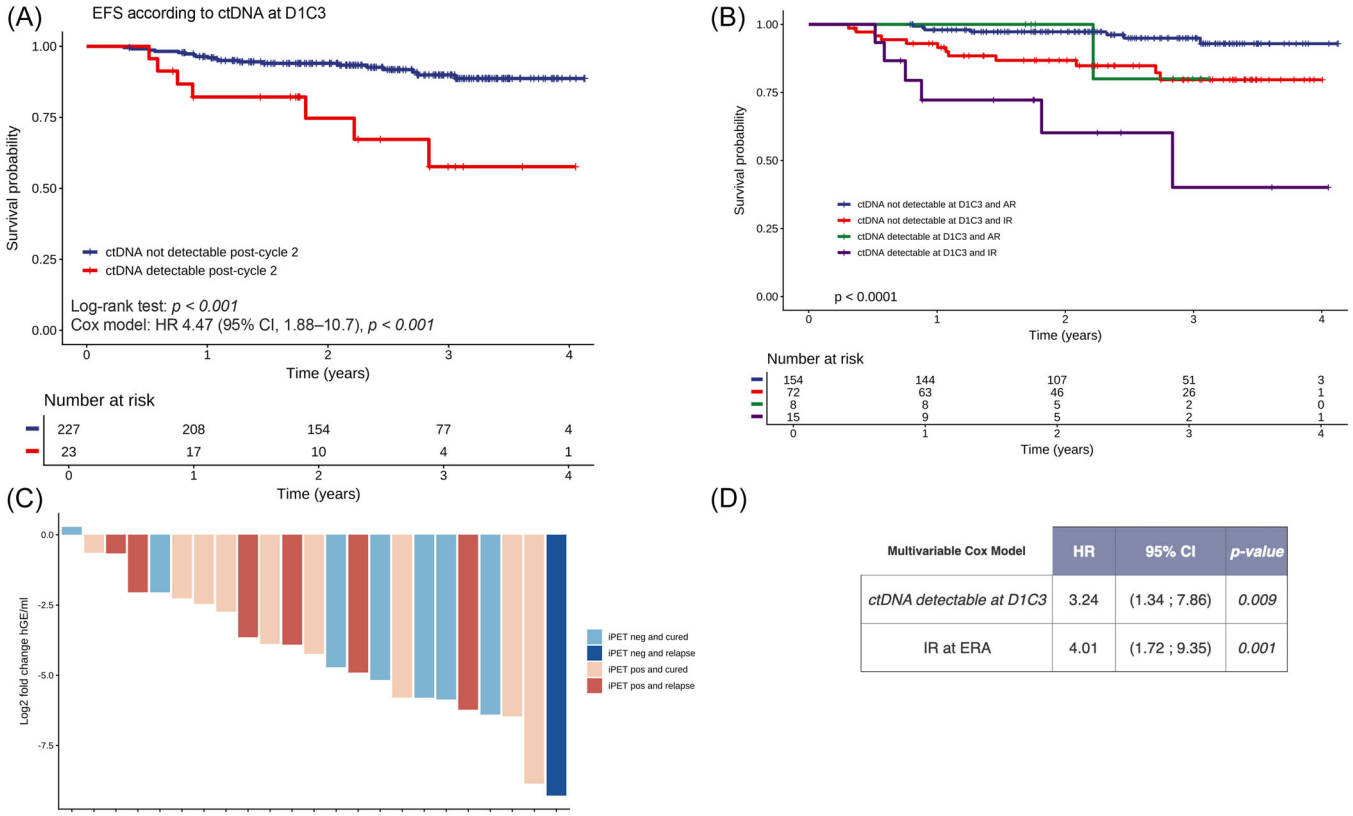

FIGURE 3 **Prognostic impact of circulating tumor DNA (ctDNA) status at D1C3 on event-free survival (EFS). (A)** Kaplan–Meier curves showing EFS according to ctDNA detectability at D1C3 (post-Cycle 2). Patients with undetectable ctDNA at D1C3 (blue, *N* = 227) had significantly superior EFS compared to patients with persistent detectable ctDNA (red, *N* = 23; log-rank P < 0.001). Univariate Cox regression confirmed the strong adverse prognostic impact of detectable ctDNA at D1C3 (hazard ratio [HR] = 4.47, 95% CI: 1.88–10.7, P < 0.001). **(B)** Kaplan–Meier curves stratifying patients by both ctDNA status at D1C3 and overall response at early response assessment (ERA). Four groups are shown: ctDNA not detectable at D1C3 with adequate response (AR, blue, *N* = 154), ctDNA not detectable at D1C3 with inadequate response (IR, red, *N* = 72), ctDNA detectable at D1C3 with AR (green, *N* = 8), and ctDNA detectable at D1C3 with IR (purple, *N* = 15). The combined stratification demonstrated significant prognostic discrimination (overall log-rank P < 0.0001). **(C)** Waterfall plot displaying the log2 fold change in ctDNA concentration (hGE/mL) from diagnosis to D1C3 in the 23 patients with persistent detectable ctDNA post-Cycle 2. Each bar represents an individual ordered ctDNA reduction. Bar colors indicate the combination of interim positron emission tomography (PET) at ERA (iPET) response and clinical outcome: iPET negative and cured (light blue), iPET negative and relapse (dark blue), iPET positive and cured (light salmon), and iPET positive and relapse (dark red). **(D)** Multivariable Cox regression analysis demonstrating independent prognostic significance of ctDNA detectability at D1C3 (HR = 3.24, 95% CI: 1.34–7.86, P = 0.009) and IR at ERA (HR = 4.01, 95% CI: 1.72–9.35, P = 0.001). Both factors remained significant predictors of inferior EFS when adjusted for each other, indicating complementary prognostic value of ctDNA monitoring and metabolic response assessment

Recent studies have provided important insights into the oncogenesis of cHL. Heger et al.[12] performed comprehensive molecular profiling in a large cohort of adult (*n* = 243) and pediatric (*n* = 96) cHL patients and proposed an oncogenetic classification based on mutational landscape and predominant oncogenic drivers with prognostic implications. Similarly, Alig et al.[11] analyzed 366 patients using ctDNA profiling and identified two genomic subtypes with distinct clinical and immunological features, including therapeutically targetable truncating IL4R mutations. Using PV enrichment sequencing (PhasED-seq), they demonstrated that both pretreatment and on-treatment ctDNA levels improved risk stratification and enabled detection of occult minimal residual disease, supporting ctDNA as a noninvasive tool for genotyping and dynamic monitoring in cHL.

In the specific context of pediatric cHL, Desch et al.[8] conducted a comprehensive analysis of tumor circulating DNA in 96 pediatric cHL patients enrolled in the German cohort of the EuroNet-PHL-C2 study. They employed a hybrid capture-targeted NGS assay capable of detecting SNVs, insertions/deletions, translocations, and VH-DH-JH rearrangements. Their findings established a significant correlation between ctDNA levels and disease burden at diagnosis. In a limited subset of patients with sequential ctDNA samples collected during therapy, they observed that persistent ctDNA was associated with poor response as evaluated by PET imaging. However, this study did not report any significant impact on EFS, potentially due to the limited sample size and follow-up duration.

Primerano et al. conducted an analysis of cfDNA in plasma samples from 155 pediatric patients with cHL.[10] Their findings revealed that patients who exhibited elevated plasma cfDNA levels following the first cycle of chemotherapy subsequently demonstrated inferior clinical outcomes. Additionally, patients who achieved complete responses with durable progression-free survival (PFS) showed a more pronounced reduction in cfDNA levels after two chemotherapy cycles compared to those who eventually experienced disease relapse. However, a significant limitation of this study was the cfDNA quantification methodology employed, which lacked the specificity to distinguish tumor-derived ctDNA from other sources of circulating DNA, potentially introducing confounding factors that complicated the interpretation of results.

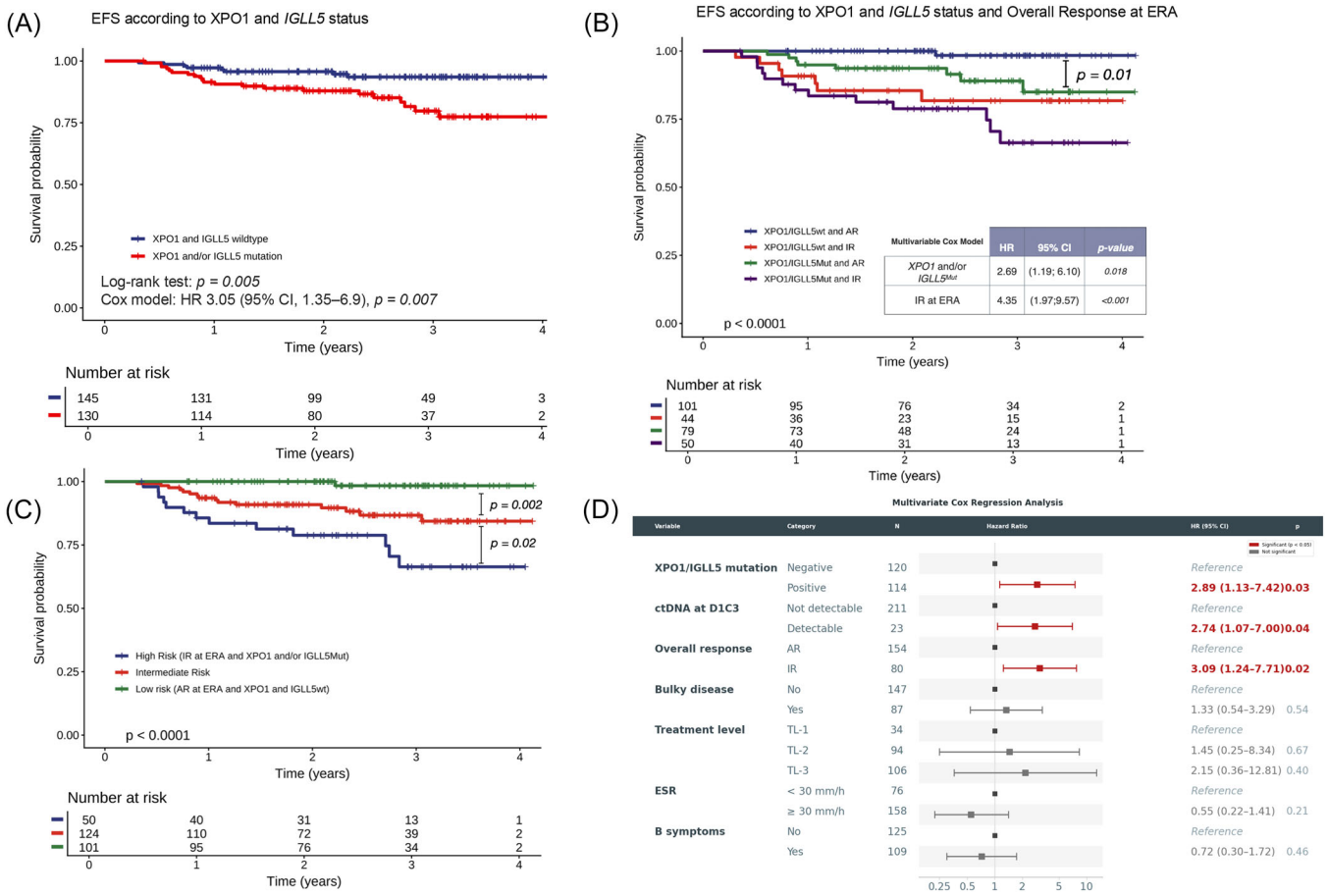

FIGURE 4 **Prognostic impact of *XPO1/IGLL5* mutational status and early response assessment on event-free survival. (A)** Kaplan–Meier curves showing event-free survival (EFS) according to *XPO1* and *IGLL5* mutational status. Patients with wild-type *XPO1* and *IGLL5* (blue, *N* = 145) had significantly better EFS compared to patients harboring *XPO1* and/or *IGLL5* mutations (red, *N* = 130; log-rank P = 0.005). Univariate Cox regression confirmed the adverse prognostic impact of *XPO1/IGLL5* mutation (HR = 3.05, 95% CI: 1.35–6.9, P = 0.007). **(B)** Kaplan–Meier curves stratifying patients by both *XPO1/IGLL5* mutational status and overall response at early response assessment (ERA). Four groups are shown: *XPO1/IGLL5* wild-type with adequate response (AR, blue, *N* = 101), *XPO1/IGLL5* wild-type with inadequate response (IR, red, *N* = 44), *XPO1/IGLL5* mutated with AR (green, *N* = 79), and *XPO1/IGLL5* mutated with IR (purple, *N* = 50). Table shows a multivariable Cox regression analysis demonstrating the independent prognostic significance of both *XPO1/IGLL5* mutation (HR = 2.69, 95% CI: 1.19–6.10, P = 0.018) and IR at ERA (HR = 4.35, 95% CI: 1.97–9.57, P < 0.001). **(C)** Risk stratification model combining *XPO1/IGLL5* mutational status and ERA response. Patients were classified into three risk groups: low risk (AR at ERA and *XPO1/IGLL5* wild-type, green, *N* = 101), intermediate risk (red, *N* = 124), and high risk (IR at ERA and *XPO1* and/or *IGLL5* mutation, blue, *N* = 50). **(D)** Forest plot displaying multivariate Cox regression analysis of prognostic factors for EFS. Variables assessed include *XPO1/IGLL5* mutation status, ctDNA detectability at D1C3, overall response (AR vs. IR), bulky disease, treatment level (TL-1, TL-2, and TL-3), ESR (≥ 30 mm/h), and B-symptoms.

Identifying mutations at diagnosis that predict treatment response and relapse remains a significant challenge in cHL. In our study, we report that *TP53* mutations (affecting 7% of the cohort) were strongly associated with both IR at ERA and LRA, yet showed no significant impact on EFS. This is likely attributable to the therapeutic intervention protocol for patients with IR at ERA in the EuroNet-PHL-C2 study. Notably, the impact of *TP53* mutations was previously documented in adult cHL cohorts and was similarly associated with poor initial response.[21] We demonstrate that combining *XPO1* and *IGLL5* mutations—two recurrently altered genes in cHL—with PET-CT evaluation at ERA enables stratification into three distinct risk groups with significantly different outcomes. If validated in independent cohorts, this combined classifier may improve early identification of patients at higher risk of relapse who could benefit from treatment intensification, while also supporting de-escalation strategies in low-risk patients. Notably, Heger et al.[12] identified *IGLL5* as one of the most frequently mutated genes within their "Oncogene-driven" molecular subgroup, underscoring its potential role in cHL pathogenesis.

More importantly, regarding ctDNA as a real-time treatment response monitor, we confirmed its significant prognostic value, demonstrating that persistent ctDNA after two chemotherapy cycles identifies a very high-risk subgroup specially when combined with PET-CT evaluation at ERA. Though small (10% of patients), this group experienced markedly inferior outcomes with an EFS of only 67% at 30 months. However, the observation that 90% of patients achieved ctDNA clearance after only two treatment cycles warrants validation using more sensitive NGS technologies sequencing approaches, to ensure accurate molecular disease monitoring and exclude false-negative results among apparent complete molecular responders or patients with undetectable ctDNA at diagnosis. A limitation of our study is the relatively restricted gene panel employed, and our technical inability to detect copy number variants affecting the 9p24 chromosomal region. This region encompasses the clinically significant PD1/PDL1 locus, which has been implicated in immune evasion mechanisms potentially driving chemotherapy resistance and disease relapse.[12,22] Future studies incorporating comprehensive

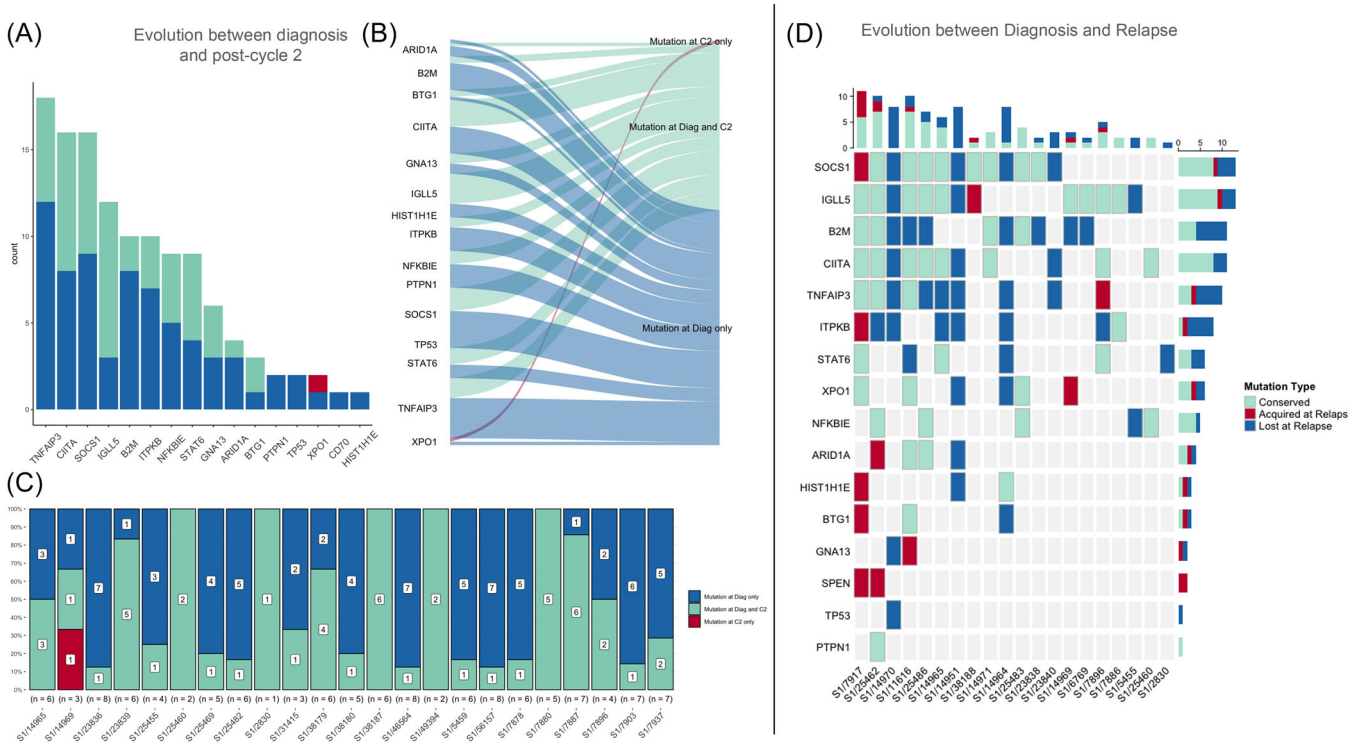

FIGURE 5 **Evolution of the mutational landscape between diagnosis, post-Cycle 2 (D1C3), and relapse. (A)** Bar chart displaying the number of mutations detected for each gene at diagnosis and/or post-Cycle 2 (D1C3). **(B)** Alluvial diagram illustrating the evolution of gene-specific mutations between diagnosis and D1C3. **(C)** Patient-level stacked bar chart showing the distribution of mutations according to their temporal dynamics. **(D)** Heatmap depicting clonal evolution between diagnosis and relapse in patients who experienced disease recurrence. Columns represent individual patients and rows represent genes. The bar chart above shows the total number of mutations per patient at relapse. Most mutations were conserved at relapse, although both acquisition and loss of mutations were observed.

genomic profiling with copy number analysis capabilities would address this limitation and potentially reveal additional molecular determinants of treatment response.

The fundamental challenge in CAYA cHL management centers on the delicate balance between maximizing cure rates while minimizing treatment-related morbidity. The significant long-term complications associated with conventional chemotherapy and radiotherapy—including secondary malignancies, cardiovascular disease, and fertility issues—necessitate more precise risk stratification approaches. In this context, ctDNA emerges as a powerful and promising biomarker with dual utility: enabling refined initial risk stratification at diagnosis and providing dynamic, real-time assessment of treatment response throughout the therapeutic course. This noninvasive approach offers the potential to personalize treatment intensity based on molecular response—sparing low-risk CAYA patients from unnecessary toxicity, while identifying those with molecularly persistent disease (undetectable by current methods) who may benefit from innovative therapies such as CPI.

ACKNOWLEDGMENTS

We sincerely thank all patients and their families for their participation in this study. The authors are also grateful to all members of the SFCE (Société Française des Cancers et des Leucémies de l'Enfant et de l'Adolescent) and the investigators at the participating centers for their valuable contributions to data and sample collection. The authors would like to thank the *Unité de Recherche Clinique de l'Est Parisien* (URC-Est) AP-HP team, including Miray Beskardes, Amel Touati, Marthe Dembele, and Laurence Berard, for their support in conducting this study. They also thank Maxime Ferreboeuf, Chaima Mrad, and Ouiza Braik from the clinical research team at Armand-Trousseau Hospital for their valuable contributions.

AUTHOR CONTRIBUTIONS

Mathieu Simonin: Conceptualization; formal analysis; supervision; writing—review and editing; writing—original draft; validation; software; data curation; resources. **Mathieu Viennot**: Methodology; validation; writing—review and editing; formal analysis; software; data curation; investigation; writing—original draft. **Stéphanie Haouy**: Writing—review and editing; resources. **Stéphane Ducassou**: Resources; writing—review and editing. **Catherine Curtillet**: Writing—review and editing; resources. **Nathalie Garnier**: Resources; writing—review and editing. **Aurélie Phulpin**: Writing—review and editing; resources. **Catherine Paillard**: Resources; writing—review and editing. **Charlotte Rigaud**: Writing—review and editing; resources. **Marie-Laure Couec**: Resources; writing—review and editing. **Liana Carausu**: Writing—review and editing; resources. **Jacinthe Bonneau**: Writing—review and editing; resources. **Isabelle Pellier**: Writing—review and editing; resources. **Melissa Barbati**: Resources; writing—review and editing. **Frédéric Millot**: Writing—review and editing; resources. **Marie-Émilie Dourthe**: Writing—review and editing; resources. **Justina Kanold**: Writing—review and editing; resources. **Pascale Schneider**: Writing—review and editing; resources. **Jean-Louis Stephan**: Writing—review and editing; resources. **Camille Leglise**: Resources; writing—review and editing. **Claire Pluchart**: Writing—review and editing; resources. **Pierre-Julien Viailly**: Writing—review

and editing; data curation; formal analysis. **Victor Michel**: Writing—review and editing; formal analysis; data curation. **Sabah Boudjemaa**: Writing—review and editing. **Bénédicte Jonca**: Writing—review and editing. **Thierry Leblanc**: Writing—review and editing; resources. **Judith Landman-Parker**: Writing—review and editing; resources; funding acquisition; investigation; conceptualization; writing—original draft; visualization; validation; methodology; supervision; project administration. **Fabrice Jardin**: Conceptualization; investigation; funding acquisition; writing—original draft; methodology; validation; visualization; writing—review and editing; data curation; supervision; project administration.

CONFLICT OF INTEREST STATEMENT

The authors declare no conflicts of interest.

DATA AVAILABILITY STATEMENT

The data that support the findings of this study are available on request from the corresponding author. The data are not publicly available due to privacy or ethical restrictions.

FUNDING

This study was funded by "Fondation Enfants Cancers Santé" and *L'AREMIG* (Association pour la Recherche et les Etudes dans les Maladies Infantiles Graves), and promoted by AP-HP (Assistance Publique–Hôpitaux de Paris).

SUPPORTING INFORMATION

Additional supporting information can be found in the online version of this article.

ORCID

Mathieu Simonin https://orcid.org/0000-0002-0448-8811
Thierry Leblanc https://orcid.org/0000-0003-2463-9346

REFERENCES

1. Brice P, de Kerviler E, Friedberg JW. Classical Hodgkin lymphoma. *Lancet Lond Engl*. Published online January 22, 2021. doi:10.1016/S0140-6736(20)32207-8
2. Mauz-Körholz C, Landman-Parker J, Balwierz W, et al. Response-adapted omission of radiotherapy and comparison of consolidation chemotherapy in children and adolescents with intermediate-stage and advanced-stage classical Hodgkin lymphoma (EuroNet-PHL-C1): a titration study with an open-label, embedded, multinational, non-inferiority, randomised controlled trial. *Lancet Oncol*. 2022;23(1):125-137. doi:10.1016/S1470-2045(21)00470-8
3. Daw S, Hasenclever D, Mascarin M, et al. Risk and response adapted treatment guidelines for managing first relapsed and refractory classical Hodgkin lymphoma in children and young people. Recommendations from the EuroNet Pediatric Hodgkin Lymphoma Group. *HemaSphere*. 2020;4(1):e329. doi:10.1097/HS9.0000000000000329
4. Steidl C, Connors JM, Gascoyne RD. Molecular pathogenesis of Hodgkin's lymphoma: increasing evidence of the importance of the microenvironment. *J Clin Oncol*. 2011;29(14):1812-1826. doi:10.1200/JCO.2010.32.8401
5. Pourmaleki M, Jones CJ, Mellinghoff SD, et al. Multiplexed spatial profiling of Hodgkin Reed-Sternberg cell neighborhoods in classic Hodgkin lymphoma. *Clin Cancer Res*. 2024;30(17):3881-3893. doi:10.1158/1078-0432.CCR-24-0942
6. Spina V, Bruscaggin A, Cuccaro A, et al. Circulating tumor DNA reveals genetics, clonal evolution, and residual disease in classical Hodgkin lymphoma. *Blood*. 2018;131(22):2413-2425. doi:10.1182/blood-2017-11-812073
7. Alcoceba M, García-Álvarez M, Chillón MC, et al. Liquid biopsy: a non-invasive approach for Hodgkin lymphoma genotyping. *Br J Haematol*. 2021;195(4):542-551. doi:10.1111/bjh.17719
8. Desch AK, Hartung K, Botzen A, et al. Genotyping circulating tumor DNA of pediatric Hodgkin lymphoma. *Leukemia*. 2020;34(1):151-166. doi:10.1038/s41375-019-0541-6
9. Camus V, Viennot M, Lequesne J, et al. Targeted genotyping of circulating tumor DNA for classical Hodgkin lymphoma monitoring: a prospective study. *Haematologica*. 2020;106(1):154-162. doi:10.3324/haematol.2019.237719
10. Primerano S, Burnelli R, Carraro E, et al. Kinetics of circulating plasma cell-free DNA in paediatric classical Hodgkin lymphoma. *J Cancer*. 2016;7(4):364-366. doi:10.7150/jca.13593
11. Alig SK, Shahrokh Esfahani M, Garofalo A, et al. Distinct Hodgkin lymphoma subtypes defined by noninvasive genomic profiling. *Nature*. 2024;625(7996):778-787. doi:10.1038/s41586-023-06903-x
12. Heger JM, Mammadova L, Mattlener J, et al. Circulating tumor DNA sequencing for biologic classification and individualized risk stratification in patients with Hodgkin lymphoma. *J Clin Oncol*. 2024;42(35):4218-4230. doi:10.1200/JCO.23.01867
13. Pirosa MC, Bruscaggin A, Terzi di Bergamo L, et al. A comprehensive genetic study of classic Hodgkin lymphoma using circulating tumor DNA. *Blood*. 2025;146(10):1207-1224. doi:10.1182/blood.2024027355
14. Medeiros LJ, Chadburn A, Natkunam Y, Naresh KN. WHO 5th Edition Classification Project. Fifth Edition of the World Health Classification of Tumors of the Hematopoietic and Lymphoid Tissues: B-cell Neoplasms. *Mod Pathol Off J U S Can Acad Pathol Inc*. 2024;37(4):100441. doi:10.1016/j.modpat.2024.100441
15. Scherer F, Kurtz DM, Newman AM, et al. Distinct biological subtypes and patterns of genome evolution in lymphoma revealed by circulating tumor DNA. *Sci Transl Med*. 2016;8(364):364ra155. doi:10.1126/scitranslmed.aai8545
16. Sater V, Viailly PJ, Lecroq T, et al. UMI-varcal: a low-frequency variant caller for UMI-tagged paired-end sequencing data. *Methods Mol Biol Clifton NJ*. 2022;2493:235-245. doi:10.1007/978-1-0716-2293-3_14
17. Claudel A, Cottereau AS, Bachy E, et al. Combined PET and ctDNA response as a predictor of POD24 for follicular lymphoma after first-line induction treatment. *Blood*. 2025;146(8):913-925. doi:10.1182/blood.2024027727
18. Tibshirani R. The LASSO method for variable selection in the Cox model. *Stat Med*. 1997;16(4):385-395. doi:10.1002/(sici)1097-0258(19970228)16:4%3C385::aid-sim380%3E3.0.co;2-3
19. Simonin M, Jardin F, Leblanc T, Latour S, Landman Parker J. An update on molecular features and therapeutic perspectives of pediatric classical Hodgkin Lymphoma. What the clinician needs to know? *Eur J Med Genet*. 2023;66(1):104672. doi:10.1016/j.ejmg.2022.104672
20. Camus V, Jardin F. Cell-free DNA for the management of classical Hodgkin lymphoma. *Pharm Basel Switz*. 2021;14(3):207. doi:10.3390/ph14030207
21. Sobesky S, Mammadova L, Cirillo M, et al. In-depth cell-free DNA sequencing reveals genomic landscape of Hodgkin's lymphoma and facilitates ultrasensitive residual disease detection. *Med N Y N*. 2021;2(10):1171-1193. doi:10.1016/j.medj.2021.09.002
22. Roemer MGM, Advani RH, Ligon AH, et al. PD-L1 and PD-L2 genetic alterations define classical Hodgkin lymphoma and predict outcome. *J Clin Oncol*. 2016;34(23):2690-2697. doi:10.1200/JCO.2016.66.4482